

LETTER TO THE EDITOR

# Reionization with star-forming galaxies: insights from the Low- $z$ Lyman Continuum Survey

M. Trebitsch<sup>1</sup>, P. Dayal<sup>1</sup>, J. Chisholm<sup>2</sup>, S. L. Finkelstein<sup>2</sup>, A. Jaskot<sup>3</sup>, S. Flury<sup>4</sup>, D. Schaerer<sup>5,6</sup>, H. Atek<sup>7</sup>, S. Borthakur<sup>8</sup>, H. Ferguson<sup>9</sup>, F. Fontanot<sup>10,11</sup>, M. Giavalisco<sup>4</sup>, A. Grazian<sup>12</sup>, M. Hayes<sup>13</sup>, F. Leclercq<sup>2</sup>, V. Mauerhofer<sup>1</sup>, G. Östlin<sup>13</sup>, A. Saldana-Lopez<sup>6</sup>, T. Thuan<sup>14</sup>, B. Wang<sup>15</sup>, G. Worseck<sup>16</sup>, and X. Xu<sup>17</sup>

<sup>1</sup> Kapteyn Astronomical Institute, University of Groningen, P.O. Box 800, 9700 AV Groningen, The Netherlands  
e-mail: m.trebitsch@rug.nl

<sup>2</sup> Department of Astronomy, The University of Texas at Austin, Austin, TX, USA

<sup>3</sup> Department of Astronomy, Williams College, Williamstown, MA 01267, United States

<sup>4</sup> INAF-Osservatorio Astronomico di Trieste, Via G.B. Tiepolo, 11, I-34143, Trieste, Italy

<sup>5</sup> Department of Astronomy, University of Geneva, 51 Chemin Pegasi, 1290 Versoix, Switzerland

<sup>6</sup> CNRS, IRAP, 14 Avenue E. Belin, 31400 Toulouse, France

<sup>7</sup> Institut d'Astrophysique de Paris, CNRS UMR7095, Sorbonne Université, 98bis Boulevard Arago, F-75014 Paris, France

<sup>8</sup> School of Earth & Space Exploration, Arizona State University, Tempe, AZ 85287, United States

<sup>9</sup> Space Telescope Science Institute, 3700 San Martin Drive Baltimore, MD 21218, United States

<sup>10</sup> INAF-Osservatorio Astronomico di Trieste, Via G.B. Tiepolo, 11, I-34143, Trieste, Italy

<sup>11</sup> IFPU-Institute for Fundamental Physics of the Universe, via Beirut 2, I-34151, Trieste, Italy

<sup>12</sup> INAF-Osservatorio Astronomico di Padova, Vicolo dell'Osservatorio 5, I-35122, Padova, Italy

<sup>13</sup> The Oskar Klein Centre, Department of Astronomy, Stockholm University, AlbaNova, SE-10691 Stockholm, Sweden

<sup>14</sup> Astronomy Department, University of Virginia, Charlottesville, VA 22904, United States

<sup>15</sup> Department of Astronomy & Astrophysics, The Pennsylvania State University, University Park, PA 16802, USA

<sup>16</sup> Institut für Physik und Astronomie, Universität Potsdam, Karl-Liebknecht-Str. 24/25, D-14476 Potsdam, Germany

<sup>17</sup> Department of Physics and Astronomy, Johns Hopkins University, Baltimore, MD 21218, United States

Received XXX; accepted YYY

## ABSTRACT

**Context.** The fraction of ionizing photons escaping from galaxies,  $f_{\text{esc}}$ , is at the same time a crucial parameter in modelling reionization and a very poorly known quantity, especially at high redshift.

**Aims.** Recent observations are starting to constrain the values of  $f_{\text{esc}}$  in low- $z$  star-forming galaxies, but the validity of this comparison remains to be verified.

**Methods.** Applying at high- $z$  the empirical relation between  $f_{\text{esc}}$  and the UV slope trends derived from the *Low- $z$  Lyman Continuum Survey*, we use the DELPHI semi-analytical galaxy formation model to estimate the global ionizing emissivity of high- $z$  galaxies, which we use to compute the resulting reionization history.

**Results.** We find that both the global ionizing emissivity and reionization history match the observational constraints. Assuming that the low- $z$  correlations hold during the epoch of reionization, we find that galaxies with  $-16 \lesssim M_{\text{UV}} \lesssim -13.5$  are the main drivers of reionization. We derive a population-averaged  $\langle f_{\text{esc}} \rangle \approx 8\%$ ,  $10\%$ ,  $20\%$  at  $z = 4.5, 6, 8$ .

**Key words.** dark ages, reionization, first stars – galaxies: high-redshift

## 1. Introduction

Over the past decade, large efforts have been made to understand the epoch of reionization (EoR) (see e.g. the recent reviews of Dayal & Ferrara 2018; Robertson 2022), during which the Lyman Continuum (LyC) photons produced by early sources ionized the neutral intergalactic medium (IGM) in around one billion years, with most of the hydrogen being reionized by  $z \lesssim 6$  (e.g. Fan et al. 2006, but see also e.g. Bosman et al. 2022). One of the key questions pertaining to the EoR is the nature of the sources of LyC photons, active galactic nuclei (AGN) or massive stars in star-forming galaxies. While deep observations start to characterize the faint AGN population, observations (e.g. Fontanot et al. 2012; Matsuoka et al. 2018; Kulkarni et al. 2019) and simulations (e.g. Qin et al. 2017; Eide et al. 2020; Dayal

et al. 2020; Trebitsch et al. 2021; Yung et al. 2021) suggest that their role is sub-dominant (but see Giallongo et al. 2015; Grazian et al. 2018, 2022), requiring the fainter but more numerous star forming galaxies to be the drivers of reionization.

One key parameter of their contribution is the fraction of LyC photons ( $f_{\text{esc}}$ ) that can escape after transfer through the interstellar medium (ISM). Unfortunately, this parameter cannot be measured directly during the EoR as the mean free path of LyC photons is too short at  $z \gtrsim 4$  (Inoue et al. 2014). The only way to directly measure  $f_{\text{esc}}$  is to use galaxies that form analogues of the sources of reionization, but at lower redshifts where LyC photons can reach us. Using ground-based optical data, several groups have been exploring analogues at  $z \gtrsim 3$  (e.g. Marchi et al. 2017; Steidel et al. 2018; Vanzella et al. 2018; Fletcher et al. 2019, although the attenuation by the IGM is not negligible at these

redshifts). Alternatively, space-based observations in the ultraviolet (UV) with the Hubble Space Telescope (HST) of  $z \sim 0.3$  compact star-forming galaxies sharing similarities with the  $z \gtrsim 6$  population (e.g. Schaerer et al. 2022) has proven extremely successful in the past few years in detecting LyC emitters (LCEs, e.g. Izotov et al. 2016b,a, 2018a,b; Wang et al. 2019; Izotov et al. 2021; Flury et al. 2022a) and exploring their physical properties (e.g. Verhamme et al. 2017; Gazagnes et al. 2020; Ramambason et al. 2020; Flury et al. 2022b; Xu et al. 2022). In particular, the recent Low- $z$  Lyman-Continuum Survey (LzLCS; PI: Jaskot, HST Project ID: 15626, Flury et al. 2022a) represent a large effort to extend the parameter space of galaxy properties probed by previous LCE samples. The LzLCS is a large HST program targeting 66 star-forming  $z \sim 0.3$  galaxies over 134 orbits using the Cosmic Origin Spectrograph (COS). Of these galaxies, 35 have a strong  $> 2\sigma$  LyC detection with  $f_{\text{esc}}$  in the range 0.1% – 20%, bringing the number of detected LCEs to 50 out of 89 targeted galaxies when combined with archival data.

We therefore need to assess how well low- $z$  analogues represent the sources of reionization. Cosmological simulations of galaxies have proved very useful in the past few years: detailed radiation hydrodynamics (RHD) simulations predict a complex, time-dependent, behaviour of  $f_{\text{esc}}$  as a function of the host galaxy properties (e.g. Paardekooper et al. 2015; Rosdahl et al. 2018; Barrow et al. 2020), suggesting in particular that the presence of stellar feedback (both radiative and mechanical) is crucial in allowing LyC photons to reach the IGM (e.g. Wise et al. 2014; Kimm & Cen 2014; Trebitsch et al. 2017). However, these simulations are extremely expensive, using tens of millions of computing hours to describe the high- $z$  population alone. Additionally, cosmological RHD simulations are only starting to reach the resolution needed to model star-forming clouds, a requirement to address this question properly (e.g. Howard et al. 2018; Kimm et al. 2019, 2022). It is therefore currently unfeasible to follow down to low redshift the properties of a large sample of galaxies at the appropriate resolution in a full RHD simulation.

In this Letter, we take an alternative approach to test the viability of using low- $z$  samples to probe the physics of the sources of reionization. We model reionization using a semi-analytical galaxy formation model, DELPHI (Dayal et al. 2014, 2022), which we combine with a correlation empirically derived from the LzLCS that relates the slope of the stellar continuum in the UV,  $\beta$ , and the escape fraction of LyC photons,  $f_{\text{esc}}$ . This allows us to extend the low- $z$  LCE properties to high- $z$ .

## 2. Coupling DELPHI to the LzLCS

### 2.1. Galaxy formation model

We model galaxy formation with the DELPHI semi-analytic model (Dayal et al. 2014, 2022). In brief, DELPHI uses a binary merger tree approach to jointly track the build-up of dark matter halos and their baryonic components (gas, stellar, metal and dust mass). This model follows the assembly histories of galaxies with halo masses in the range  $M_{\text{vir}} = 10^8 - 10^{14} M_{\odot}$  from  $z \sim 40$  down to  $z = 4.5$ . The available gas mass (from both mergers and IGM accretion) can form stars with an effective star formation efficiency  $f_{\text{eff}}^* = \min[f_{\text{ej}}^*, f_*]$ , which is the minimum between the efficiency that produces enough SNII energy to eject the remainder of the gas ( $f_{\text{ej}}^*$ ) and an upper maximum threshold ( $f_*$ ) which is one of our free parameters. In ionized regions, the UV radiation will suppress star formation e.g. by photo-evaporating low-mass haloes or reduce their gas inflows (e.g. Dawoodbhoj et al. 2018; Katz et al. 2019; Ocvirk et al. 2020,

for recent simulations). We model the coupling between the ionizing UV background and galaxy formation as in Dayal et al. (2020) by assuming full photo-evaporation of gas in low-mass haloes with  $M_{\text{vir}} \leq M_{\text{crit}}$ , preventing them from forming stars. In this work, we explore the case of no UV suppression as well as  $M_{\text{crit}} = 10^{8.5}, 10^9, 10^{9.5} M_{\odot}$ , with the intermediate value being our fiducial case. The choice of this value is motivated by the results of the RHD CoDA simulation (Ocvirk et al. 2020) and the semi-numerical ASTRÆUS model (Hutter et al. 2021), where haloes below that mass show a suppressed star formation. We do not include AGN in this model as we explored their role within the DELPHI framework in Dayal et al. (2020).

The dust model is described in Dayal et al. (2022), so we only summarize its main features here. We include the key processes of production, astration, destruction of dust into metals, ejection, and dust grain growth in the ISM (that leads to a corresponding decrease in the metal mass) to calculate the total dust mass  $M_d$  and metal mass  $M_Z$  for each galaxy. The model predicts a dust-to-metal ratio of the order of 30% – 40% for our galaxies, consistent with low-metallicity DLA observations (De Cia et al. 2013; Wiseman et al. 2017). We use this dust mass to infer the dust optical depth to UV continuum by assuming that the dust and gas are co-spatially distributed in a disk of radius  $r_g = 4.5\lambda r_{\text{vir}}$  (e.g. Ferrara et al. 2000), where  $r_{\text{vir}}$  is the virial radius and  $\lambda = 0.04$  (e.g. Davis & Natarajan 2009) is the spin parameter of the halo. Assuming a dust grain size of  $a = 0.05 \mu\text{m}$  and a mass density of  $s = 2.25 \text{ g.cm}^{-3}$  appropriate for a mixture of graphite and carbonaceous grains (Todini & Ferrara 2001; Nozawa et al. 2003), this leads to a dust optical depth  $\tau_d = 3M_d/(4\pi r_g^2 a s)$  with a dust extinction efficiency  $Q_{\text{ext}} = 1$  at  $1500 \text{ \AA}$ . Assuming that stars, gas, and dust are intermixed in the disk locally modelled as a slab, we can write the fraction of UV that is absorbed by the disk as  $1 - f_c$ , where

$$f_c = \frac{1 - e^{-\tau_d}}{\tau_d}. \quad (1)$$

Our model contains only two mass- and redshift-independent parameters to match observations: the maximum (instantaneous) star formation efficiency of  $f_* = 8\%$  and the fraction  $f_w (\approx 7.5\%)$  of the SNII energy available to drive an outflow. These parameters have been tuned to simultaneously reproduce the  $z \sim 5 - 12$  stellar mass functions (González et al. 2011; Duncan et al. 2014; Song et al. 2016) and UV luminosity function (Castellano et al. 2010; McLure et al. 2013; Atek et al. 2015; Finkelstein et al. 2015; Bouwens et al. 2016; Calvi et al. 2016; Bowler et al. 2017; Livermore et al. 2017; Ishigaki et al. 2018; Oesch et al. 2018; Bouwens et al. 2021; Harikane et al. 2022, LF), with the luminosity (UV and ionizing) being inferred from STARBURST99 templates (Leitherer et al. 1999) using the metallicity and the star formation history using a Kroupa (2001) initial mass function between  $0.1 - 100 M_{\odot}$ , after attenuation by dust using Eq. 1.

### 2.2. Escape fraction

We now describe how we infer the escape fraction  $f_{\text{esc}}$  of each galaxy as a function of its (attenuated) UV luminosity. We follow the results of Chisholm et al. (2022) who used the LzLCS sample consolidated with a selection of other LCEs taken from the literature (Izotov et al. 2016b,a, 2018a,b; Wang et al. 2019; Izotov et al. 2021) for a total of 89 galaxies.

With this extended sample, Chisholm et al. (2022) used the spectral fitting approach of Saldana-Lopez et al. (2022b) to reconstruct the stellar populations properties (burst ages and metallicities) of these low- $z$  galaxies, and derived the spectral slope in

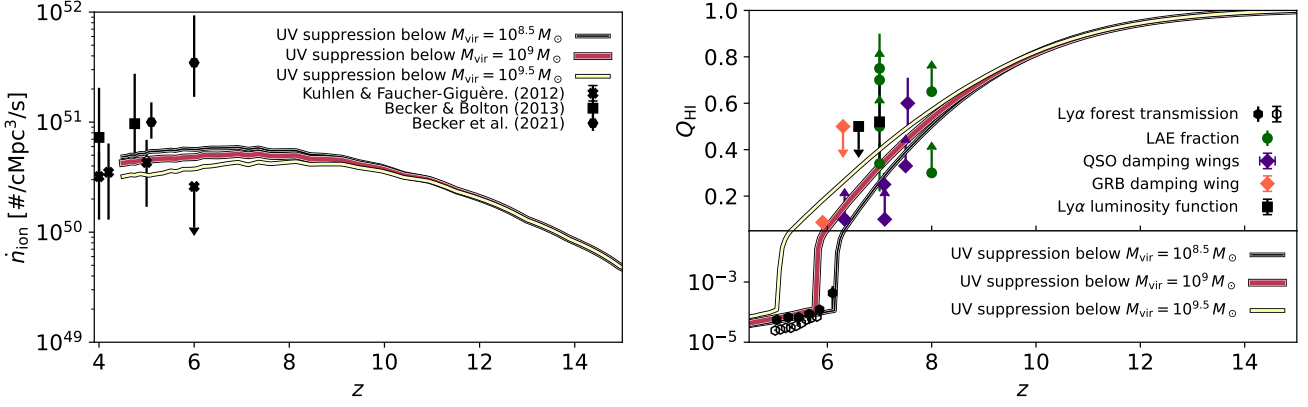


**Fig. 1.** *Left:* Global ionizing photon emission rate for our fiducial model (thick red line) and for the low and high suppression models (yellow and black thin lines, respectively), compared to the observations of [Kuhlen & Faucher-Giguère \(2012\)](#), crosses) [Becker & Bolton \(2013\)](#), squares), and [Becker et al. \(2021\)](#), hexagons). *Right:* H I volume filling fraction for the same models, compared to observations: black hexagons for measurements of the Lyman- $\alpha$  forest transmission from [Fan et al. \(2006\)](#), full symbols) and [Bosman et al. \(2022\)](#), open symbols); green circles for constraints on the IGM opacity from the fraction of Lyman- $\alpha$  emitters in Lyman-break galaxy samples ([Schenker et al. 2014](#); [Ono et al. 2012](#); [Pentericci et al. 2014](#); [Robertson et al. 2013](#); [Tilvi et al. 2014](#)); purple diamonds for measurements from quasar damping wings ([Mortlock et al. 2011](#); [Schroeder et al. 2013](#); [Bañados et al. 2018](#); [Đurovičková et al. 2020](#)); orange diamonds for gamma-ray bursts constraints ([Totani et al. 2006, 2016](#)); and the black squares are constraints derived from the evolution of the Lyman- $\alpha$  luminosity function by [Ouchi et al. \(2010\)](#); [Ota et al. \(2008\)](#). Some of these points have been taken from compilation of [Bouwens et al. \(2015\)](#).

the range 1300 – 1800 Å centred on 1550 Å,  $\beta$ , from the inferred spectra. Combining  $\beta$  with the  $f_{\text{esc}}$  measured from the consolidated LzLCS sample, [Chisholm et al. \(2022\)](#) derived the following relation including non-LCEs as upper limits:

$$f_{\text{esc}} = (1.3 \pm 0.6) \times 10^{-4} \times 10^{(-1.22 \pm 0.1)\beta}. \quad (2)$$

We adopt this relation between the LyC  $f_{\text{esc}}$  and the UV properties of the galaxies, and proceed to connect these  $\beta$  slopes to the UV luminosity of the galaxies predicted by DELPHI. As our goal is to apply this to the high- $z$  population, we choose to adopt a  $\beta$ – $M_{\text{UV}}$  relation directly derived from high- $z$  samples rather than the LzLCS one: indeed, as  $\beta$  is strongly related to the dust content of galaxies, the resulting  $f_{\text{esc}}$ – $M_{\text{UV}}$  relation will incorporate the properties of high- $z$  dust. While this comes at the cost of full self-consistency, [Chisholm et al. \(2022\)](#) show that the LzLCS sample follows the same  $\beta$ – $M_{\text{UV}}$  trend as at high- $z$ . We use the  $\beta$ – $M_{\text{UV}}$  relation of [Bouwens et al. \(2014\)](#), see also [Finkelstein et al. 2012](#); [Dunlop et al. 2013](#)), which can be written as:

$$\beta = \beta_{19.5}(z) + \frac{d\beta}{dM_{\text{UV}}}(M_{\text{UV}} + 19.5), \quad (3)$$

where  $\beta_{19.5} = \beta(M_{\text{UV}} = -19.5)$ . We fit the evolution of  $\beta_{19.5}(z)$  from [Bouwens et al. \(2014\)](#) with a first order polynomial, and fix the slope to  $-0.125$ , the best-fit constant value:

$$\beta = -1.993 - 0.071(z - 6) - 0.125(M_{\text{UV}} + 19.5). \quad (4)$$

Injecting Eq. 4 in Eq. 2, we get a relation between the UV luminosity of a galaxy (from DELPHI) and its  $f_{\text{esc}}$ . At fixed  $M_{\text{UV}}$ ,  $f_{\text{esc}}$  increases slightly with increasing redshift: from  $\approx 3\%$  (12%) at  $z = 6$  to  $\approx 6.5\%$  (19%) at  $z = 10$  for  $M_{\text{UV}} = -20$  (–16). We further choose to limit the minimum value of the slope to  $\beta = -2.6$ , similar to the bluest slopes observed in the LzLCS sample and consistent with the bluest slopes found at high- $z$  ([Finkelstein et al. 2012](#); [Bouwens et al. 2014](#)), corresponding to  $f_{\text{esc}} \approx 20\%$ .

### 2.3. Reionization model

We can now compute the evolution of the volume filling fraction of ionized hydrogen,  $Q_{\text{HII}} = 1 - Q_{\text{HI}}$ , following the updated “reionization equation” approach of [Madau \(2017, Eq. 24\)](#):

$$\frac{dQ_{\text{HII}}}{dt} = \frac{\dot{n}_{\text{ion}}}{\langle n_{\text{H}} \rangle (1 + \langle \kappa_{\nu_L}^{\text{LLS}} \rangle / \langle \kappa_{\nu_L}^{\text{IGM}} \rangle)} - \frac{Q_{\text{HII}}}{\bar{t}_{\text{rec}}}, \quad (5)$$

where  $\dot{n}_{\text{ion}}$  is the emission rate of ionizing photons into the IGM,  $\langle n_{\text{H}} \rangle$  is the mean density of hydrogen, and  $\bar{t}_{\text{rec}} = 1 / [(1 + \chi) \langle n_{\text{H}} \rangle \alpha_0 C_R]$  is the effective recombination timescale in the IGM.  $\bar{t}_{\text{rec}}$  depends on  $\alpha_0$  the case-A recombination coefficient (taken at  $T_0 = 10^{4.3}$  K) and on the clumping factor  $C_R = 2.9 [(1 + z)/6]^{-1.1}$  from [Shull et al. \(2012\)](#), and  $\chi = 0.083$ . Finally,  $\langle \kappa_{\nu_L}^{\text{LLS}} \rangle$  and  $\langle \kappa_{\nu_L}^{\text{IGM}} \rangle$  are the volume-averaged absorption probabilities per unit length due to Lyman-limit systems and the uniform IGM, respectively ([Madau 2017, Eq. 11 and Eq. 13\).](#)

In this work, we use our DELPHI runs described in Sect. 2.1 to estimate the intrinsic ionizing photon production rate of each galaxy ( $\dot{N}_{\text{ion}}^{\text{int}}$ , in photons/s) and its escape fraction  $f_{\text{esc}}$  based on its  $M_{\text{UV}}$ . The total ionizing photon emission rate  $\dot{n}_{\text{ion}}$  is then given by the sum of the contribution coming from all haloes, weighted by the halo mass function  $\phi(M)$ . We account for the effect of UV radiation on galaxies in ionized regions by using our “photo-suppressed” models for a fraction  $Q_{\text{HII}}$  of the galaxies, and the case without UV suppression for the remaining fraction  $Q_{\text{HI}}$ , as in, e.g. [Choudhury & Dayal \(2019\)](#). Formally:

$$\dot{n}_{\text{ion}} = \int_{M_{\text{vir}}} f_{\text{esc}} [\dot{N}_{\text{UVsup}}^{\text{int}} Q_{\text{HII}} + \dot{N}_{\text{noUVsup}}^{\text{int}} Q_{\text{HI}}] \phi(M) dM. \quad (6)$$

This expression depends non-trivially on  $Q_{\text{HII}}$ , so that solving Eq. 5 effectively takes into account the radiative feedback on the galaxy population. In practice, we solve Eq. 5 using a backward differentiation formula method with SCIPY’s OdeSolver<sup>1</sup>.

<sup>1</sup> <https://scipy.org/>

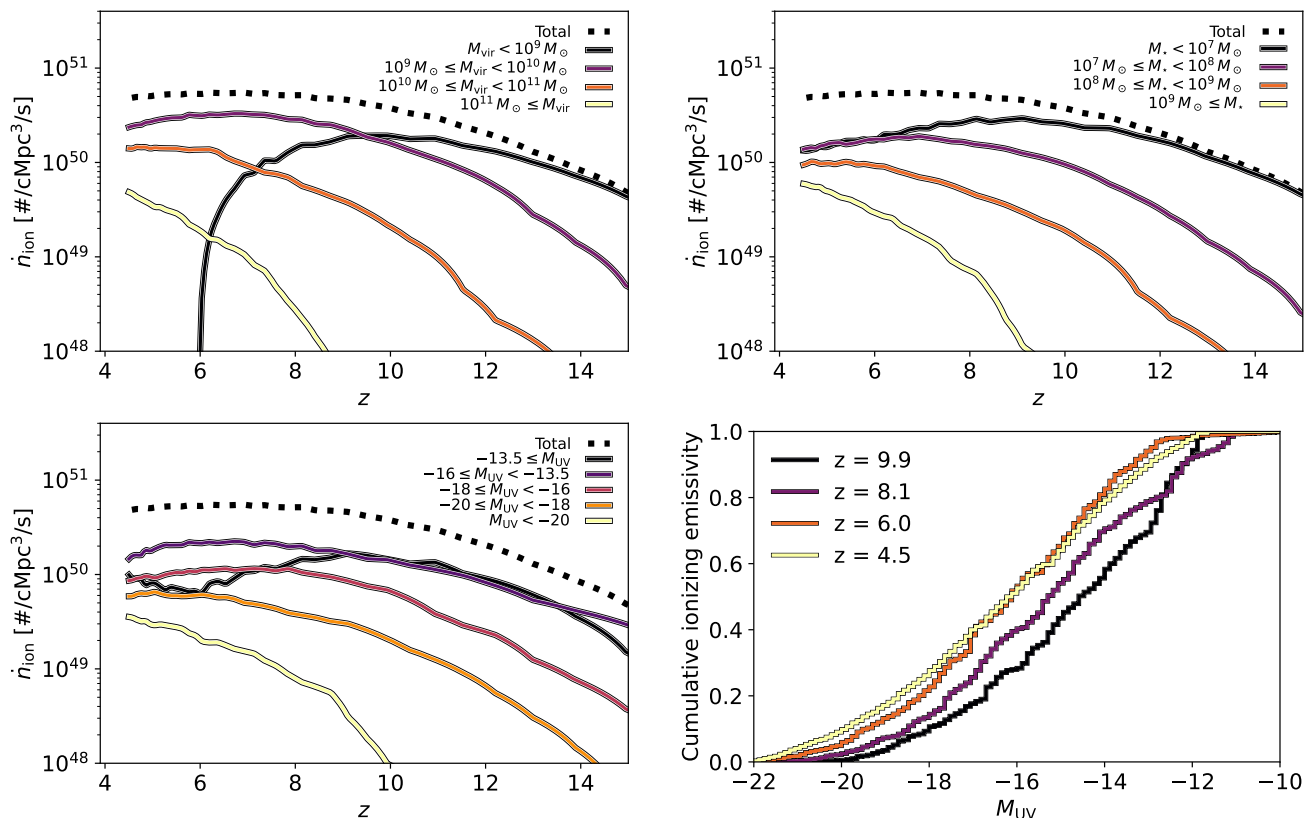


**Fig. 2.** Evolution of the ionizing emission rate for our fiducial model for the whole galaxy population (dotted line) and for haloes of different total mass (*top left*), stellar mass (*top right*), and observed UV magnitude (*bottom left*). The *bottom right* panel shows the cumulative emissivity as a function of observed  $M_{UV}$ . Reionization is driven by relatively low-mass and faint galaxies in haloes with masses  $10^9 M_{\odot} \leq M_{vir} < 10^{10} M_{\odot}$ .

### 3. Results

#### 3.1. Global reionization

We present in Fig. 1 the main results from our modelling: the left panel shows the evolution of  $\dot{n}_{ion}$  as a function of redshift for our fiducial model (in red), where star formation is suppressed in haloes with  $M_{vir} \leq 10^9 M_{\odot}$  in ionized regions, and the models with UV suppression below  $10^{8.5} M_{\odot}$  and  $10^{9.5} M_{\odot}$  are shown in black and yellow, respectively. As expected, when the critical mass for UV suppression increases, the total emissivity decreases: this is directly due to the fact that fewer galaxies contribute to the total emissivity, with our most suppressed model producing approximately half as many photons as the least suppressed one at  $z \lesssim 8$ . The photo-suppression only plays a role in suppressing galaxies when the UV background is well established (i.e.  $Q_{HII} \approx 1$ ), only causing minor differences in  $\dot{n}_{ion}$ . All three models predict an emissivity consistent with the observations from Becker & Bolton (2013, black squares), but on the lower end of the allowed range: this is most likely because we do not include AGN in this model, while they start to make a significant contribution at  $z \lesssim 4.5$  (Finkelstein et al. 2019; Dayal et al. 2020; Trebitsch et al. 2021).

The resulting reionization history is shown in the right panel of Fig. 1, comparing our model to a selection of observational constraints (see caption). Our fiducial model reproduces best all observational constraints: the model with the strongest UV suppression lacks the ionizing photons to complete reionization in time, while the model with a low critical mass reionizes the Universe just too early. The post-overlap behaviour of our model is

mostly dictated by the inclusion of the  $\langle \kappa_{VL}^{LLS} \rangle$  term, designed to reproduce the  $z < 5.5$  forest, so the agreement with the Fan et al. (2006) points is not surprising. Overall, we find that if the LyC trends from the LzLCS can be extended to high- $z$ , our model suggests (without specific tuning) that galaxies alone can reionize the Universe by  $z \lesssim 6$ .

#### 3.2. Which galaxies are the main drivers of reionization?

Having established that our model reproduces reasonably well the global reionization history, we can use it to probe the physics of the sources of reionization. We show in Fig. 2 a breakdown of the contributions to  $\dot{n}_{ion}$  from different galaxy population for our fiducial model, sorted by halo mass (top left), stellar mass (top right), and observed UV luminosity (bottom left). In all three panels, the dashed line indicate the total  $\dot{n}_{ion}$ . The ionizing budget is dominated at early times by the lowest mass haloes, with  $M_{vir} < 10^9 M_{\odot}$ , but their contribution drops as they are more and more photo-suppressed, becoming negligible at  $z \lesssim 6$  when reionization is complete. During the majority of the reionization era ( $6 \lesssim z \lesssim 9$ ), the haloes with masses  $10^9 M_{\odot} \leq M_{vir} < 10^{10} M_{\odot}$  represent the main contributors to  $\dot{n}_{ion}$  ( $\sim 60\%$  at  $z \approx 8$ ). Grouping galaxies by stellar mass yields a similar behaviour: at  $z \geq 10$ , the galaxies with  $M_{\star} < 10^7 M_{\odot}$  dominate as they live in haloes that are not yet photo-suppressed. Their contribution then decreases, but remains dominant: this is mostly because as more massive haloes get partly photo-suppressed, they will host galaxies in that stellar mass bin while contributing to  $\dot{n}_{ion}$  (see e.g. Hutter et al. 2021). By the end of reionization, galaxies with masses

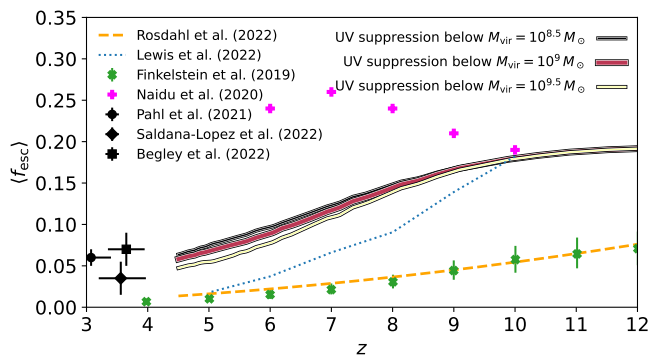


**Fig. 3.** Evolution of the luminosity-weighted, population-averaged  $f_{\text{esc}}$  for our three models: we find a slow decrease from  $\langle f_{\text{esc}} \rangle \simeq 20\%$  at  $z \geq 10$  to  $\langle f_{\text{esc}} \rangle \simeq 8\%$  at  $z \simeq 4$ . The extrapolation of our model to lower redshift aligns well with observational constraints (e.g. Pahl et al. 2021; Saldana-Lopez et al. 2022a; Begley et al. 2022, black points), and is in qualitative agreement with the trend found by models (Finkelstein et al. 2019; Naidu et al. 2020, green and pink crosses) and simulations (Rosdahl et al. 2022, orange dashed line), close to the simulation of Lewis et al. (2022, blue dotted line).

$10^7 M_{\odot} \leq M_{\star} < 10^8 M_{\odot}$  contribute as much as this lowest mass bin, and galaxies with  $10^8 M_{\odot} \leq M_{\star} < 10^9 M_{\odot}$  contribute almost as much. This suggests an intermediate pathway between the “reionization by the faintest galaxies” (e.g. Finkelstein et al. 2019) and the “reionization by rare galaxies” (e.g. Naidu et al. 2020) scenarios. Finally, we find that at  $6 \lesssim z \lesssim 9$  galaxies with  $-16 \lesssim M_{\text{UV}} \lesssim -13.5$  drive reionization. By comparison, the galaxies fainter than  $M_{\text{UV}} = -13.5$  only play an important role at the beginning of reionization, with their contribution remaining similar to that of galaxies with  $-18 \lesssim M_{\text{UV}} \lesssim -16$  and  $-20 \lesssim M_{\text{UV}} \lesssim -18$  at later time as a result of UV suppression, and the brightest galaxies remain subdominant throughout the reionization era. We show in the bottom right panel of Fig. 2 the cumulative contribution to  $\dot{n}_{\text{ion}}$  as a function of observed  $M_{\text{UV}}$ : the contribution of faint galaxies decreases as reionization progresses, with the contribution from galaxies brighter than  $M_{\text{UV}} = -15$  evolving from  $\simeq 40\%$  at  $z \simeq 10$  to over  $60\%$  at  $z \lesssim 6$ .

This paints a picture that contrasts with the empirical results of e.g. Naidu et al. (2020), whose model suggests that relatively bright galaxies contribute significantly, while here they only contribute at late time. This discrepancy mainly comes from different assumptions for the behaviour of  $f_{\text{esc}}$  with galaxy properties: Naidu et al. (2020) implement a model where more massive galaxies have a higher  $f_{\text{esc}}$ , driven by the idea that stronger feedback carves holes more efficiently in the ISM, as advocated e.g. by Sharma et al. (2016); they further assume a relatively shallow UV LF, leading to a lower contribution of low-luminosity sources. By contrast, our observationally motivated  $f_{\text{esc}}$  model yields a higher  $f_{\text{esc}}$  for faint, low-mass galaxies, in better agreement with recent RHD simulations (e.g. Katz et al. 2019; Lewis et al. 2020; Rosdahl et al. 2022). With our model, the bulk of the reionizing population from Naidu et al. (2020) ( $M_{\text{UV}} < -18$ ) has  $\beta > -2.2$ , and so  $f_{\text{esc}} < 8\%$ . Nevertheless, while our model suggests that faint galaxies drive reionization, it is less extreme that the Finkelstein et al. (2019) scenario, where the faintest galaxies are responsible for reionization.

A key prediction of the Naidu et al. (2020) and Finkelstein et al. (2019) empirical models is the evolution of the global  $f_{\text{esc}}$  with redshift. Driven by the evolution of the faint-end slope of the UV luminosity function, Finkelstein et al. (2019) find that

$f_{\text{esc}}$  decreases with increasing cosmic time, while Naidu et al. (2020) find the opposite. We show in Fig. 3 our luminosity-weighted, population-averaged  $f_{\text{esc}}$  with the same colour-coding as Fig. 1. At  $z \geq 9 - 10$ , the global  $\langle f_{\text{esc}} \rangle$  saturates around  $20\%$ , our maximum value, before decreasing at lower  $z$ : this is because the lowest mass haloes dominate the very early emissivity, while they get photo-suppressed as reionization proceeds. Again, we qualitatively agree with Finkelstein et al. (2019), albeit with quantitative differences: at  $z \simeq 4.5, 6, 8$ , we find  $\langle f_{\text{esc}} \rangle \simeq 8\%, 10\%, 20\%$ , compared to  $\lesssim 1\%, 2\%, 5\%$  in their model. This slow decrease of  $\langle f_{\text{esc}} \rangle$  is in good agreement with  $z \simeq 3$  observations and upper limits (e.g. Guaita et al. 2016; Steidel et al. 2018; Meštrić et al. 2021; Pahl et al. 2021; Begley et al. 2022; Saxena et al. 2022; Saldana-Lopez et al. 2022a) which have  $f_{\text{esc}} \lesssim 10\%$  (Begley et al. 2022, but see also Rivera-Thorsen et al. 2022), suggesting at face value that LzLCS galaxies exhibit LyC properties broadly similar to the high- $z$  galaxy population. While RHD simulations usually stop before  $z \simeq 3$ , the trend of  $\langle f_{\text{esc}} \rangle$  decreasing with lower redshift is a common feature: Rosdahl et al. (2018, 2022) find that  $\langle f_{\text{esc}} \rangle$  goes from  $\simeq 12 - 15\%$  at  $z \simeq 15$  to  $\simeq 3 - 8\%$  at  $z = 6$ , in qualitative agreement with our model. Similarly, Trebitsch et al. (2021) find a decreasing  $\langle f_{\text{esc}} \rangle$  in the OBELISK simulation down to values close to  $\simeq 2 - 3\%$  at  $z \simeq 4$ , while Lewis et al. (2022) and the Alt6 model of Dayal et al. (2020) find an evolution of  $f_{\text{esc}}$  with  $z$  very similar to ours.

#### 4. Summary

In this Letter we have combined the semi-analytical galaxy formation model DELPHI with observations of low- $z$  LyC emitters from the (consolidated) LzLCS. By relating the escape of LyC photons with the UV properties of the host galaxy, we have built a simple but consistent model for the reionization of the Universe. Our main results are as follow:

- A direct application of the  $f_{\text{esc}} - \beta$  relation found in the LzLCS to galaxies in the EoR yield a reasonable population of sources of ionizing photons. Using these sources to solve the reionization equation matches current observational constraints on the reionization history.
- The faintest galaxies in the lowest mass haloes dominate the early stages of reionization, but become sub-dominant at  $z \lesssim 9$  when they become photo-suppressed by the UV background that becomes more prevalent.
- At the end of reionization, galaxies with  $-16 \lesssim M_{\text{UV}} \lesssim -13.5$ , which will be observable with the JWST, are dominating the LyC budget, while the brightest galaxies with  $M_{\text{UV}} < -20$  are sub-dominant at all times.
- The average  $\langle f_{\text{esc}} \rangle$  decreases over time, going from  $\langle f_{\text{esc}} \rangle \simeq 20\%$  at  $z \geq 8$  to  $\langle f_{\text{esc}} \rangle \simeq 8\%$  at  $z \simeq 4$ , in qualitative agreement with the predictions of high-resolution RHD simulations and observations at  $z \geq 3$ .

These results demonstrate the power of using observations of low- $z$  galaxies with a strategy such as that of the LzLCS to get insights on the population of galaxies deep in the reionization epoch, and pave the way for more detailed models and comparisons with high- $z$  samples.

*Acknowledgements.* MT thanks J. Lewis for sharing results from the DUSTIER simulation. MT, PD, and VM acknowledge support from the NWO grant 0.16.VIDI.189.162 (“ODIN”). PD acknowledges support from University of Groningen’s CO-FUND Rosalind Franklin Program. ASL acknowledge support from Swiss National Science Foundation. This work has made extensive use of the NASA’s Astrophysics Data System, as well as the MATPLOTLIB (Hunter 2007), NUMPY/SCIPY (Harris et al. 2020) and IPYTHON (Perez & Granger 2007) packages.

This research is based on observations made with the NASA/ESA Hubble Space Telescope obtained from the Space Telescope Science Institute, which is operated by the Association of Universities for Research in Astronomy, Inc., under NASA contract NAS 5–26555. These observations are associated with program HST-GO-15626.

## References

- Atek, H., Richard, J., Jauzac, M., et al. 2015, *ApJ*, 814, 69
- Bañados, E., Venemans, B. P., Mazzucchelli, C., et al. 2018, *Nature*, 553, 473
- Barrow, G. S. S., Robertson, B. E., Ellis, R. S., et al. 2020, *ApJ*, 902, L39
- Becker, G. D. & Bolton, J. S. 2013, *MNRAS*, 436, 1023
- Becker, G. D., D’Aloisio, A., Christenson, H. M., et al. 2021, *MNRAS*, 508, 1853
- Begley, R., Cullen, F., McLure, R. J., et al. 2022, *MNRAS*, 513, 3510
- Bosman, S. E. I., Davies, F. B., Becker, G. D., et al. 2022, *MNRAS*, 514, 55
- Bouwens, R. J., Aravena, M., Decarli, R., et al. 2016, *ApJ*, 833, 72
- Bouwens, R. J., Illingworth, G. D., Oesch, P. A., et al. 2015, *ApJ*, 811, 140
- Bouwens, R. J., Illingworth, G. D., Oesch, P. A., et al. 2014, *ApJ*, 793, 115
- Bouwens, R. J., Oesch, P. A., Stefanon, M., et al. 2021, *AJ*, 162, 47
- Bowler, R. A. A., Dunlop, J. S., McLure, R. J., & McLeod, D. J. 2017, *MNRAS*, 466, 3612
- Calvi, V., Trenti, M., Stiavelli, M., et al. 2016, *ApJ*, 817, 120
- Castellano, M., Fontana, A., Paris, D., et al. 2010, *A&A*, 524, A28
- Chisholm, J., Saldana-Lopez, A., Flury, S., et al. 2022, *MNRAS*, 517, 5104
- Choudhury, T. R. & Dayal, P. 2019, *MNRAS*, 482, L19
- Davis, A. J. & Natarajan, P. 2009, *MNRAS*, 393, 1498
- Dawoodbhoj, T., Shapiro, P. R., Ocvirk, P., et al. 2018, *MNRAS*, 480, 1740
- Dayal, P. & Ferrara, A. 2018, *Phys. Rep.*, 780, 1
- Dayal, P., Ferrara, A., Dunlop, J. S., & Pacucci, F. 2014, *MNRAS*, 445, 2545
- Dayal, P., Ferrara, A., Sommovigo, L., et al. 2022, *MNRAS*, 512, 989
- Dayal, P., Volonteri, M., Choudhury, T. R., et al. 2020, *MNRAS*, 495, 3065
- De Cia, A., Ledoux, C., Savaglio, S., Schady, P., & Vreeswijk, P. M. 2013, *A&A*, 560, A88
- Duncan, K., Conselice, C. J., Mortlock, A., et al. 2014, *MNRAS*, 444, 2960
- Dunlop, J. S., Rogers, A. B., McLure, R. J., et al. 2013, *MNRAS*, 432, 3520
- Eide, M. B., Ciardi, B., Graziani, L., et al. 2020, *MNRAS*, 498, 6083
- Fan, X., Strauss, M. A., Becker, R. H., et al. 2006, *AJ*, 132, 117
- Ferrara, A., Pettini, M., & Shchekinov, Y. 2000, *MNRAS*, 319, 539
- Finkelstein, S. L., D’Aloisio, A., Paardekooper, J.-P., et al. 2019, *ApJ*, 879, 36
- Finkelstein, S. L., Papovich, C., Salmon, B., et al. 2012, *ApJ*, 756, 164
- Finkelstein, S. L., Ryan, Russell E., J., Papovich, C., et al. 2015, *ApJ*, 810, 71
- Fletcher, T. J., Tang, M., Robertson, B. E., et al. 2019, *ApJ*, 878, 87
- Flury, S. R., Jaskot, A. E., Ferguson, H. C., et al. 2022a, *ApJS*, 260, 1
- Flury, S. R., Jaskot, A. E., Ferguson, H. C., et al. 2022b, *ApJ*, 930, 126
- Fontanot, F., Cristiani, S., & Vanzella, E. 2012, *MNRAS*, 425, 1413
- Gazagnes, S., Chisholm, J., Schaerer, D., Verhamme, A., & Izotov, Y. 2020, *A&A*, 639, A85
- Giallongo, E., Grazian, A., Fiore, F., et al. 2015, *A&A*, 578, A83
- González, V., Labbé, I., Bouwens, R. J., et al. 2011, *ApJ*, 735, L34
- Grazian, A., Giallongo, E., Boutsia, K., et al. 2022, *ApJ*, 924, 62
- Grazian, A., Giallongo, E., Boutsia, K., et al. 2018, *A&A*, 613, A44
- Guaita, L., Pentericci, L., Grazian, A., et al. 2016, *A&A*, 587, A133
- Harikane, Y., Ono, Y., Ouchi, M., et al. 2022, *ApJS*, 259, 20
- Harris, C. R., Millman, K. J., van der Walt, S. J., et al. 2020, *Nature*, 585, 357
- Howard, C. S., Pudritz, R. E., Harris, W. E., & Klessen, R. S. 2018, *MNRAS*, 475, 3121
- Hunter, J. D. 2007, *Computing in Science and Engineering*, 9, 90
- Hutter, A., Dayal, P., Yepes, G., et al. 2021, *MNRAS*, 503, 3698
- Inoue, A. K., Shimizu, I., Iwata, I., & Tanaka, M. 2014, *MNRAS*, 442, 1805
- Ishigaki, M., Kawamata, R., Ouchi, M., et al. 2018, *ApJ*, 854, 73
- Izotov, Y. I., Orlitová, I., Schaerer, D., et al. 2016a, *Nature*, 529, 178
- Izotov, Y. I., Schaerer, D., Thuan, T. X., et al. 2016b, *MNRAS*, 461, 3683
- Izotov, Y. I., Schaerer, D., Worseck, G., et al. 2018a, *MNRAS*, 474, 4514
- Izotov, Y. I., Worseck, G., Schaerer, D., et al. 2021, *MNRAS*, 503, 1734
- Izotov, Y. I., Worseck, G., Schaerer, D., et al. 2018b, *MNRAS*, 478, 4851
- Katz, H., Kimm, T., Haehnelt, M. G., et al. 2019, *MNRAS*, 483, 1029
- Kimm, T., Bieri, R., Geen, S., et al. 2022, *ApJS*, 259, 21
- Kimm, T., Blaizot, J., Garel, T., et al. 2019, *MNRAS*, 486, 2215
- Kimm, T. & Cen, R. 2014, *ApJ*, 788, 121
- Kroupa, P. 2001, *MNRAS*, 322, 231
- Kuhlen, M. & Faucher-Giguère, C.-A. 2012, *MNRAS*, 423, 862
- Kulkarni, G., Worseck, G., & Hennawi, J. F. 2019, *MNRAS*, 488, 1035
- Leitherer, C., Schaerer, D., Goldader, J. D., et al. 1999, *ApJS*, 123, 3
- Lewis, J. S. W., Ocvirk, P., Aubert, D., et al. 2020, *MNRAS*, 496, 4342
- Lewis, J. S. W., Ocvirk, P., Dubois, Y., et al. 2022, *arXiv e-prints*, arXiv:2204.03949
- Livermore, R. C., Finkelstein, S. L., & Lotz, J. M. 2017, *ApJ*, 835, 113
- Madau, P. 2017, *ApJ*, 851, 50
- Marchi, F., Pentericci, L., Guaita, L., et al. 2017, *A&A*, 601, A73
- Matsuoka, Y., Strauss, M. A., Kashikawa, N., et al. 2018, *ApJ*, 869, 150
- McLure, R. J., Dunlop, J. S., Bowler, R. A. A., et al. 2013, *MNRAS*, 432, 2696
- Meštrić, U., Ryan-Weber, E. V., Cooke, J., et al. 2021, *MNRAS*, 508, 4443
- Mortlock, D. J., Warren, S. J., Venemans, B. P., et al. 2011, *Nature*, 474, 616
- Naidu, R. P., Tacchella, S., Mason, C. A., et al. 2020, *ApJ*, 892, 109
- Nozawa, T., Kozasa, T., Umeda, H., Maeda, K., & Nomoto, K. 2003, *ApJ*, 598, 785
- Ocvirk, P., Aubert, D., Sorce, J. G., et al. 2020, *MNRAS*, 496, 4087
- Oesch, P. A., Bouwens, R. J., Illingworth, G. D., Labbé, I., & Stefanon, M. 2018, *ApJ*, 855, 105
- Ono, Y., Ouchi, M., Mobasher, B., et al. 2012, *ApJ*, 744, 83
- Ota, K., Iye, M., Kashikawa, N., et al. 2008, *ApJ*, 677, 12
- Ouchi, M., Shimasaku, K., Furusawa, H., et al. 2010, *ApJ*, 723, 869
- Paardekooper, J.-P., Khochfar, S., & Dalla Vecchia, C. 2015, *MNRAS*, 451, 2544
- Pahl, A. J., Shapley, A., Steidel, C. C., Chen, Y., & Reddy, N. A. 2021, *MNRAS*, 505, 2447
- Pentericci, L., Vanzella, E., Fontana, A., et al. 2014, *ApJ*, 793, 113
- Perez, F. & Granger, B. E. 2007, *Computing in Science and Engineering*, 9, 21
- Qin, Y., Mutch, S. J., Poole, G. B., et al. 2017, *MNRAS*, 472, 2009
- Ramambanson, L., Schaerer, D., Stasińska, G., et al. 2020, *A&A*, 644, A21
- Rivera-Thorsen, T. E., Hayes, M., & Melinder, J. 2022, *A&A*, 666, A145
- Robertson, B. E. 2022, *ARA&A*, 60, 121
- Robertson, B. E., Furlanetto, S. R., Schneider, E., et al. 2013, *ApJ*, 768, 71
- Rosdahl, J., Blaizot, J., Katz, H., et al. 2022, *MNRAS*, 515, 2386
- Rosdahl, J., Katz, H., Blaizot, J., et al. 2018, *MNRAS*, 479, 994
- Saldana-Lopez, A., Schaerer, D., Chisholm, J., et al. 2022a, *arXiv e-prints*, arXiv:2211.01351
- Saldana-Lopez, A., Schaerer, D., Chisholm, J., et al. 2022b, *A&A*, 663, A59
- Saxena, A., Pentericci, L., Ellis, R. S., et al. 2022, *MNRAS*, 511, 120
- Schaerer, D., Marques-Chaves, R., Barrufet, L., et al. 2022, *A&A*, 665, L4
- Schenker, M. A., Ellis, R. S., Konidaris, N. P., & Stark, D. P. 2014, *ApJ*, 795, 20
- Schroeder, J., Mesinger, A., & Haiman, Z. 2013, *MNRAS*, 428, 3058
- Sharma, M., Theuns, T., Frenk, C., et al. 2016, *MNRAS*, 458, L94
- Shull, J. M., Harness, A., Trenti, M., & Smith, B. D. 2012, *ApJ*, 747, 100
- Song, M., Finkelstein, S. L., Ashby, M. L. N., et al. 2016, *ApJ*, 825, 5
- Steidel, C. C., Bogosavljević, M., Shapley, A. E., et al. 2018, *ApJ*, 869, 123
- Tilvi, V., Papovich, C., Finkelstein, S. L., et al. 2014, *ApJ*, 794, 5
- Todini, P. & Ferrara, A. 2001, *MNRAS*, 325, 726
- Totani, T., Aoki, K., Hattori, T., & Kawai, N. 2016, *PASJ*, 68, 15
- Totani, T., Kawai, N., Kosugi, G., et al. 2006, *PASJ*, 58, 485
- Trebtsch, M., Blaizot, J., Rosdahl, J., Devriendt, J., & Slyz, A. 2017, *MNRAS*, 470, 224
- Trebtsch, M., Dubois, Y., Volonteri, M., et al. 2021, *A&A*, 653, A154
- Vanzella, E., Nonino, M., Cupani, G., et al. 2018, *MNRAS*, 476, L15
- Đurovičková, D., Katz, H., Bosman, S. E. I., et al. 2020, *MNRAS*, 493, 4256
- Verhamme, A., Orlitová, I., Schaerer, D., et al. 2017, *A&A*, 597, A13
- Wang, B., Heckman, T. M., Leitherer, C., et al. 2019, *ApJ*, 885, 57
- Wise, J. H., Demchenko, V. G., Halicek, M. T., et al. 2014, *MNRAS*, 442, 2560
- Wiseman, P., Schady, P., Bolmer, J., et al. 2017, *A&A*, 599, A24
- Xu, X., Henry, A., Heckman, T., et al. 2022, *ApJ*, 933, 202
- Yung, L. Y. A., Somerville, R. S., Finkelstein, S. L., et al. 2021, *MNRAS*, 508, 2706